

Reduced-Quantum-Uncertainty States for an Atomic Clock

Monika H. Schleier-Smith, Ian D. Leroux, and Vladan Vuletić*

Department of Physics, MIT-Harvard Center for Ultracold Atoms, and Research Laboratory of Electronics, Massachusetts Institute of Technology, Cambridge, Massachusetts 02139, USA

(Dated: May 8, 2022)

Many of the most accurate measurements of physical quantities are performed on ensembles of particles with discrete quantum mechanical levels[1, 2, 3, 4, 5, 6, 7]. When the particles in the ensemble are uncorrelated, the measurement precision is limited by the projection noise associated with the random measurement outcomes for the individual particles[3, 8, 9]. This is known as the standard quantum limit (SQL). However, it is possible to induce quantum mechanical correlations (entanglement) between the particles to generate reduced-uncertainty states (“squeezed states”[10, 11, 12, 13, 14, 15, 16, 17, 18, 19, 20]) that, when used as input states to the measurement sequence, overcome the SQL[8, 9, 10, 15, 19]. Here we demonstrate that an optical quantum non-demolition (QND) measurement[13] can generate a squeezed input state for an atomic clock. We verify the entanglement of 5×10^4 ^{87}Rb atoms by comparing the observed reduction in projection noise (up to 9.4(8) dB) with the accompanying reduction in signal, finding sufficient squeezing to allow a 3.2(8) dB improvement in clock precision over the SQL.

In a typical precision experiment with a two-level system, formally described as a (pseudo-)spin $s = 1/2$, the energy difference between the two states is measured as a quantum mechanical phase accumulated in a given time. The result is read out as a population difference that can be formally viewed as the z -component S_z of the ensemble spin vector $\mathbf{S} = \sum_i \mathbf{s}_i$, where the sum is over the individual particles. For a given $|\mathbf{S}|^2 = S(S+1)$, the projection noise variance $(\Delta S_z)^2$ in the minimum-uncertainty unentangled (coherent) state is $(\Delta S_z)^2 = S/2$. Entanglement can reduce the quantum noise of S_z below this value by redistributing it to another spin component that does not directly affect the experiment precision. Such “spin squeezing” requires an interaction between the particles[11].

A wide range of interactions can be exploited to suppress spin noise. In atomic Bose-Einstein condensates (BECs), repulsive atom-atom interaction can suppress population fluctuations in traps with multiple minima, as indicated by anti-squeezing in a periodic potential[21] and evidenced by lengthened coherence time in a double-well system[22]. In a dilute atomic system, interaction can instead be introduced by collective coupling of the ensemble to a light field[13]. Under appropriate conditions, the light-atom interaction entangles the ensemble spin \mathbf{S} with the electromagnetic field, and a subsequent measurement of the field can then project the atomic ensemble into a spin-squeezed state[13, 17, 18]. Such a QND measurement has been used to suppress the pro-

jection noise $(\Delta S_z)^2$ of rotating [23] and stationary [24] spins.

Spin noise suppression $(\Delta S_z)^2 < S_0/2$, where $S_0 = N_0/2$ is the maximum possible spin of the ensemble containing N_0 particles, is only a necessary but not a sufficient condition for spin squeezing. On its own, it implies neither entanglement nor enhanced measurement sensitivity. For example, an ensemble where each atom is prepared in a definite s_z eigenstate has no spin noise ($(\Delta S_z)^2 = 0 < S_0/2$) and yet is unentangled; it also has no coherence ($|\langle S_x \rangle| = |\langle S_y \rangle| = 0$) and hence no clock signal. To verify and quantify spin squeezing[11], one must measure the length of the mean spin vector as well as the spin noise[8, 9]. For a mean ensemble spin vector $\langle \mathbf{S} \rangle$ oriented along the x axis, a state is spin squeezed[11, 17] along the z -direction if the variance $(\Delta S_z)^2$ obeys

$$(\Delta S_z)^2 < |\langle S_x \rangle| / 2. \quad (1)$$

A maximally coherent system with $|\langle S_x \rangle| \approx S_0$ is thus spin squeezed if the variance $(\Delta N)^2$ of the population difference $N = N_2 - N_1 = 2S_z$ between the two states $|1\rangle, |2\rangle$ satisfies $(\Delta N)^2 < N_0$. However, in real systems coherence (i.e. interference contrast) is often reduced such that $|\langle S_x \rangle| < S_0$. While spin noise suppression alone has sometimes been referred to as “squeezing,” we reserve the term for states which obey equation (1) (up to a coordinate rotation) and are therefore entangled[11, 17].

Spin-squeezed states are therefore characterized by values of the parameter $\zeta_{\text{KU}} = 2(\Delta S_z)^2 / |\langle S_x \rangle| < 1$. The first spin squeezing, with $\zeta_{\text{KU}}^{-1} \geq 0.06(2)$ dB, was achieved in room-temperature vapor by absorption of squeezed light[14]; the first two-mode spin squeezing ($\zeta_{\text{KU}}^{-1} = 1.9(5)$ dB) by a QND measurement on a light beam that had interacted with two ensembles [16]. Two ions have been entangled to yield a squeezed state[15] with $\zeta_{\text{KU}}^{-1} = 1.9(1)$ dB, and spectroscopic sensitivity has been further improved by deeper entanglement (not adequately described by the spin mean and variance) of three ions[19]. Very recently, spin squeezing with a BEC in a multiple-well potential with $\zeta_{\text{KU}}^{-1} \sim 5$ dB has been reported [25].

Improvement in spectroscopic sensitivity due to spin squeezing is quantified by the factor $\zeta_{\text{W}} = 2(\Delta S_z)^2 S_{\text{in}} / (|\langle S_x \rangle|^2)$ by which the entanglement reduces the squared noise-to-signal ratio $(\Delta S_z)^2 / |\langle S_x \rangle|^2$ below the value $1/(2S_{\text{in}})$ observed in measurements on the initial uncorrelated state with ensemble spin S_{in} [9]. To date, demonstrated improvements in spectroscopic sensitivity over the SQL are $\zeta_{\text{W}}^{-1} = 3.2(1)$ dB in the three-ion system; $\zeta_{\text{W}}^{-1} \sim 4$ dB by light-induced squeezing within

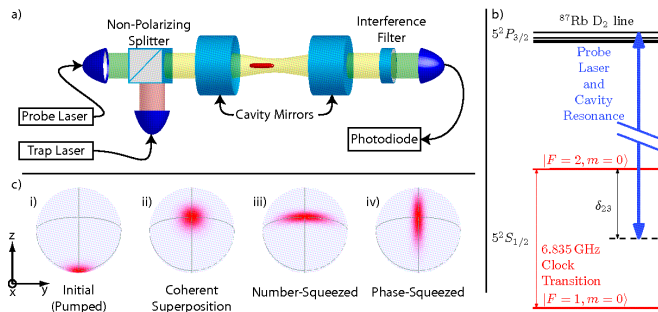


FIG. 1: **Measurement-induced pseudo-spin squeezing on an atomic clock transition.** (a) **Setup.** A laser-cooled ensemble of ^{87}Rb atoms is loaded into a far-detuned optical dipole trap inside a Fabry-Pérot resonator. The ensemble can be prepared in a quantum mechanical superposition of hyperfine clock states $|1\rangle, |2\rangle$ by microwave pulses. A population difference N produces a resonator frequency shift that is measured with a probe laser. (b) **Atomic level structure.** The resonator is tuned such that atoms in the two clock states produce equal and opposite resonator frequency shifts via the state-dependent atomic index of refraction. (c) **Preparing a squeezed input state for an atomic clock.** A number-squeezed state (iii) can be generated from a CSS along x (ii) by measurement of $S_z = N/2$. It can then be rotated by a microwave pulse into a phase-squeezed state (iv), allowing a more precise determination of the phase acquired in the free evolution time of the atomic clock.

individual atoms of large spin $s = 3$, without entanglement between the atoms[26]; and $\zeta_{\text{W}}^{-1} = 3.8(4)$ for the Bose-Einstein condensate in a periodic potential[25].

Seeking a scalable approach to squeezing that can be applied to atomic clocks and other interferometric devices using dilute atomic ensembles, we adapt the proposal by Kuzmich, Bigelow, and Mandel[13] for a QND measurement of S_z with far off-resonant light[16, 23, 24, 27]. The resulting conditionally spin-squeezed state, serving as an input state to an atomic clock, can enhance the sensitivity[13, 20] provided that one uses the information obtained in the field measurement to correct either the clock signal (post-processing) or the ensemble state (feedback)[12]. Because the light-induced squeezing profits from a large opacity (resonant optical depth OD) of the ensemble[13, 18], we use an optical resonator to enhance the optical depth from a single-pass value $OD_1 \sim 1$, typical of a standard atomic clock or atom interferometer[1, 3, 4, 5, 6], to a resonator-enhanced value $OD_r \sim 9000$, which ultimately allows much larger squeezing.

Our experiments are performed on an ensemble containing up to 5×10^4 laser-cooled ^{87}Rb atoms optically trapped inside the resonator (Fig. 1). One resonator mode is tuned such that the state-dependent atomic index of refraction produces a mode frequency shift ω that is proportional to the population difference N between the hyperfine clock states $|1\rangle = |5^2S_{1/2}, F=1, m_F=0\rangle$ and $|2\rangle = |5^2S_{1/2}, F=2, m_F=0\rangle$. The mode frequency shift per atom $d\omega/dN$ is determined from our accurately

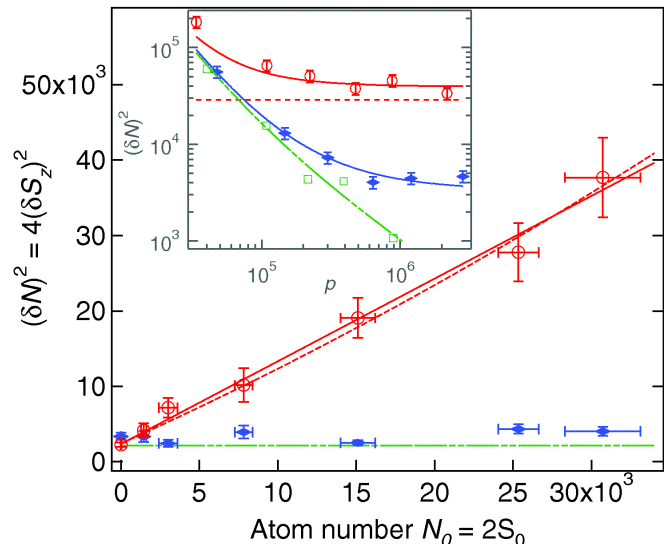


FIG. 2: **Projection noise limit and spin noise suppression.** The measured spin noise for an uncorrelated state (CSS, open red circles) agrees with the theoretical prediction $(\Delta S_z)^2 = aS_0/2$ (solid red line). The fitted slope $a^f = 1.1(1)$ is slightly higher than the prediction $a^c = 0.93(1)$ (calculated in the Supplementary Methods) due to technical noise at large atom number. If we fix $a = a^c = 0.93$ and fit this quadratic technical noise, we find a small contribution $(\delta S_z)_{\text{tech}}^2 = 6(4) \times 10^{-6} N_0^2 \ll N_0$ (dashed red curve). Our measurement of S_z , at photon number $p = 5 \times 10^5$, has an uncertainty $(\delta S_z)^2$ (solid blue diamonds) substantially below the SQL. **Inset:** Dependence of spin measurement variance $(\delta S_z)^2 = (\delta N)^2/4$ on probe photon number p for $N_0 = 3 \times 10^4$. With increasing photon number, the measurement uncertainty (solid blue diamonds) drops below the projection noise level $(\Delta S_z)_{\text{CSS}}^2 = aS_0/2$ (dashed red line), while the variance measured for independently prepared CSSs (open red circles) approaches $(\Delta S_z)_{\text{CSS}}^2$. Also shown is the technical noise without atoms expressed as an equivalent spin noise (open green squares).

measured resonator parameters and confirmed experimentally by measurement of the dual effect, namely the energy shift of the atomic levels by the intracavity light (see Methods). Given $d\omega/dN$, a measurement of ω via the transmission of a probe pulse tuned to the slope of the resonator mode yields $N = 2S_z$. Repeating such measurements reveals the average spin $\langle S_z \rangle$ and measurement variance $(\delta S_z)^2$.

We begin by experimentally verifying the projection noise level for the coherent spin state (CSS) of an uncorrelated ensemble [8, 9, 23]. As a function of (effective) atom number $N_0 = 2S_0$ (see Methods), projection noise is characterized by a variance $(\delta S_z)^2 \propto N_0$, while for technical noise $(\delta S_z)^2 \propto N_0^2$. Note that we have a reliable and accurate absolute calibration of the atom number via the resonator shift and can not only test the linear dependence $(\delta S_z)^2 \propto N_0$, as is typically done[16, 23], but also compare the slope to a calculated value that takes into account the spatially inhomogeneous coupling be-

tween the trapped atoms and the probe light. Fig. 2 shows the dependence of variance $(\delta N)^2 = 4(\delta S_z)^2$ on atom number $N_0 = 2S_0$ (open red circles). The dependence is indeed linear and the slope a agrees well with the predicted value. This confirms that we have a system dominated by projection noise and quantitatively establishes the SQL.

We now prepare a state with (conditionally) reduced S_z noise simply by measuring S_z for a CSS along x with a photon number sufficiently large to resolve S_z beyond the CSS variance $(\Delta S_z)_{\text{CSS}}^2 = S_0/2$. This measurement with variance $(\delta S_z)^2$ prepares a state with a random but known value of S_z whose quantum uncertainty is $(\Delta S_z)^2 = (\delta S_z)^2 (\Delta S_z)_{\text{CSS}}^2 / ((\Delta S_z)_{\text{CSS}}^2 + (\delta S_z)^2)$. (Throughout this letter, $(\delta S_z)^2$ refers to a measured variance, while $(\Delta S_z)^2$ denotes a quantum variance for the prepared pure or mixed state; see Supplementary Methods). The faithfulness of the state preparation is verified with a second measurement, and we plot the variance of the two measurements $(\delta N)^2 = 4(\delta S_z)^2$ vs. atom number N_0 in Fig. 2 (solid blue diamonds). While at low atom number the measurement noise exceeds the SQL due to photon shot noise and some technical noise (dash-dotted green line in Fig. 2), at higher atom number $N_0 = 3 \times 10^4$ we achieve a 9.4(8) dB suppression of spin noise below the SQL.

The reduction of $(\Delta S_z)^2$ below the SQL is accompanied by a substantial increase in $(\Delta S_y)^2$. The shape of the uncertainty region can be verified by rotating the state prepared by the squeezing pulse by a variable angle α about $\langle \mathbf{S} \rangle$ before performing the second S_z measurement. The variance $(\delta S_\alpha)^2$ thus obtained is displayed in Fig. 3. The data are well described by a model that assumes the spin noise after the first measurement to constitute an ellipse with its short axis along z (solid blue line).

Having established that we can prepare states with spin noise $(\Delta S_z)^2$ below the projection limit $S_0/2$, we need to verify whether the system remains sufficiently coherent to guarantee entanglement ($\zeta_{\text{KU}} < 1$). Fig. 4 shows the squeezing parameter $\zeta_{\text{KU}} = 2(\Delta S_z)^2 / (a|\langle S_x \rangle|)$ as a function of the number p of photons used in the state-preparation measurement. (The correction factor $a = 0.93(1)$ associated with inhomogeneous atom-light coupling is explained in the Supplementary Methods.) For $p = 3 \times 10^5$, we achieve $\zeta_{\text{KU}}^{-1} = 4.2(8)$ dB of spin squeezing. We emphasize that in this analysis we use the full observed noise, including photon shot noise and all technical noise, and all reduction in contrast $\mathcal{C} = |\langle \mathbf{S} \rangle|/S_0$, including contrast loss due to the resonator locking light (evident as finite contrast $\mathcal{C}_{\text{in}} = 0.7$ for $p = 0$ probe photons in Fig. 4). \mathcal{C}_{in} can be improved by choosing a larger detuning from atomic resonance for the lock light. The contrast reduction due to the probe light (see Supplementary Methods) is probably due to a motion-induced fluctuation of the differential light shift between the clock states, and it

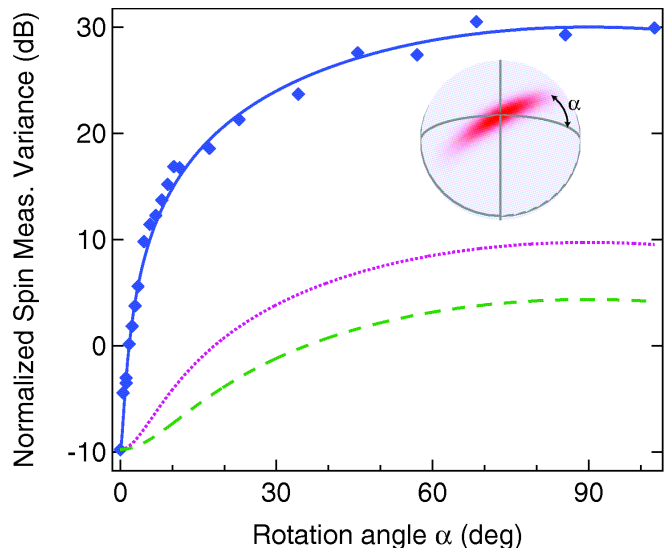


FIG. 3: **Shape of the squeezed uncertainty region.** A rotation about the mean spin vector $\langle \mathbf{S} \rangle$ is applied between the first and second spin measurements. The spin noise suppression along z ($\alpha = 0$) below the projection noise limit is accompanied by a substantial spin noise increase in the equatorial plane ($\alpha = \pi/2$). The solid blue line corresponds to an elliptic shape of the uncertainty region. The dotted magenta line would correspond to a state at the Heisenberg limit in the ideal case where the measurement does not reduce the length of the spin vector $|\mathbf{S}|$. The dashed green line is the true Heisenberg limit for our measurement, taking into account the reduction of $|\mathbf{S}|$. The uncertainty area $A = \Delta S_z \Delta S_y$ is well above the Heisenberg limit $A_H = |\mathbf{S}|/2$ (dashed green line). The larger uncertainty is primarily due to the atom-projection-noise-induced resonator shift, which produces fluctuations in probe transmission well above the photon shot noise limit, resulting in substantial differential light shifts between the clock states. This effect, though not currently a limitation on our squeezing performance, can be reduced in future experiments by measuring on cavity resonance[27] or by using a feedback technique[12].

should be possible to reduce it by cooling the atoms below the current temperature of 300 μK . The fundamental limit for our scheme, associated with photon scattering into free space, is set by the resonator-enhanced optical depth $OD_r \sim 9000$ of the ensemble and will be reached at $\zeta_{\text{KU}}^{-1} \sim 18$ dB of spin squeezing.

In our system, the ensemble without squeezing has $S_{\text{in}} = S_0 \mathcal{C}_{\text{in}}$, so that the spectroscopic improvement parameter $\zeta_{\text{W}} = 2(\Delta S_z)^2 S_{\text{in}} / (a|\langle S_x \rangle|^2)$ (including the inhomogeneity correction factor a) reduces to $\zeta_{\text{W}} = \zeta_{\text{KU}} \mathcal{C}_{\text{in}} / \mathcal{C}$. This parameter, also plotted in Fig. 4, shows an improvement in clock precision of $\zeta_{\text{W}}^{-1} = 3.2(8)$ dB.

For the data presented above, the entanglement was verified after 500 μs . The phase coherence time of the unsqueezed CSS in our current trap is 10(2) ms.

As a proof of principle, we have used the prepared squeezed state to achieve readout noise below the SQL in a Ramsey type atomic clock with a short 70 μs

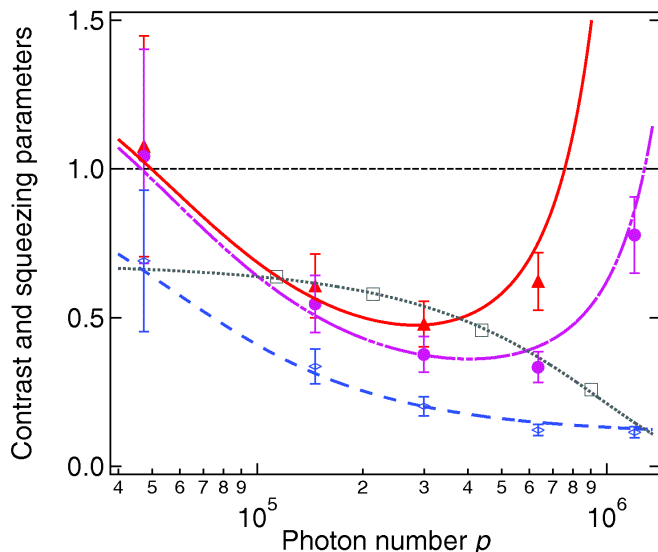


FIG. 4: **Spin noise suppression, loss of contrast, and spin squeezing.** The reduction of normalized spin noise $(\Delta S_z)^2 / (\Delta S_z)_{\text{CSS}}^2$ (blue open diamonds and dashed curve) below unity is accompanied by a loss of coherence observable as a reduced contrast \mathcal{C} (grey open squares and dotted curve) in a Ramsey clock sequence. From these two measurements, we can deduce two squeezing parameters (see text), $\zeta_{\text{KU}} = 2(\Delta S_z)^2 / (a|\langle S_x \rangle|)$ (magenta solid circles and chain-dotted curve), which characterizes the entanglement of the squeezed state, and $\zeta_{\text{W}} = 2(\Delta S_z)^2 S_{\text{in}} / (a|\langle S_x \rangle|^2)$ (red solid triangles and solid curve). The reduction of ζ_{W} below unity quantifies the squeezing-induced improvement in clock performance.

precession time. We have not yet attempted to optimize the baseline (unsqueezed) performance of this clock. However, clocks with long coherence times have already been demonstrated in magnetically trapped samples of rubidium[28, 29], a system to which our method is directly applicable. Standard ^{87}Rb fountain clocks can also operate at sufficiently high atomic density to benefit from our technique[30], as can optical-transition atomic clocks[4, 5]. It should further be possible to apply this squeezing technique to atom interferometers[6] and other precision experiments with atomic ensembles.

The group of E. Polzik has independently and simultaneously achieved results similar to ours in a Mach-Zehnder interferometer[31].

I. METHODS

We use a near-confocal Fabry-Pérot resonator which, at the 780 nm wavelength of the probe light, has a finesse $F = 5.6(2) \times 10^3$, a linewidth $\kappa = 2\pi \times 1.01(3)\text{MHz}$, and a mode waist size $w = 56.9(4) \mu\text{m}$ (much greater than the $8.1(8) \mu\text{m}$ cloud radius) at the position of the atoms.

The coupling between atom and standing-wave probe light varies with position. We therefore define an effective atom number $N_0 \equiv \frac{4\bar{\eta}}{3\eta_0} N_{\text{tot}}$ where $\bar{\eta}$ is the spatially-averaged coupling of the atoms to the probe light, η_0 is the coupling for an atom on axis at an antinode, and N_{tot} is the total number of real atoms in the cloud. The definition is chosen such that an ensemble of atoms uniformly distributed on the resonator axis obeys the usual projection-noise relation $a \equiv (\Delta N)^2 / N_0 = 1$. The small radial extent of our cloud introduces an additional correction such that $a^c = 0.93(1)$.

From the cavity parameters and our probe detuning $3.57(1) \text{GHz}$ to the blue of the $F = 2 \rightarrow F' = 3$ transition we calculate a mode frequency shift $d\omega/dN$ of $2\pi \times 48(2) \text{Hz}$ for every effective atom of population difference between the clock states. The dual effect of this differential shift is the differential Stark shift of the clock states by the probe light. We have measured it directly, finding a $250(20) \mu\text{rad}$ phase shift per probe photon for an atom at an antinode. The agreement with the $253(8) \mu\text{rad}$ calculated value confirms our quantitative understanding of the atom-light interaction in our system.

Each measurement of S_z employs two light pulses of duration $50 \mu\text{s}$, much longer than the resonator decay time $\tau = \kappa^{-1} = 158 \text{ns}$, with a $280 \mu\text{s}$ delay between them. Each pulse contains 10^5 to 10^6 photons which, after traversing the atom-resonator system, are detected with an overall quantum efficiency $Q_e = 0.43(4)$. A frequency stabilization system for probe laser and resonator ensures that the probe transmission noise is close to the photocurrent shot-noise limit. A microwave π pulse sequence between the two probe pulses suppresses the effect of the inhomogeneous Stark shifts they induce (spin echo sequence).

To reduce the effect of trap loading fluctuations when determining the projection noise limit, we perform a CSS preparation and measurement sequence (consisting of optical pumping into state $|1\rangle$, $\pi/2$ pulse, and measurement of S_z) twice with the same loaded atoms and determine the variance $(\delta S_z)^2$ between the two measurements, typically from a sample of 50 shots.

For further details see the Supplementary Methods.

II. ACKNOWLEDGEMENTS

We thank J.K. Thompson, M.D. Lukin, D. Stamper-Kurn, and E. Polzik for interesting discussions. This work was supported in part by the NSF, DARPA, and the NSF Center for Ultracold Atoms. M. S. acknowledges support from the Hertz Foundation Daniel Stroeck Fellowship and NSF. I. D. L. acknowledges support from NSERC.

-
- [1] Weiss, D. S., Young, B. C. & Chu, S. Precision measurement of the photon recoil of an atom using atomic interferometry. *Phys. Rev. Lett.* **70**, 2706–2709 (1993).
- [2] Udem, T. *et al.* Phase-coherent measurement of the hydrogen $1S - 2S$ transition frequency with an optical frequency interval divider chain. *Phys. Rev. Lett.* **79**, 2646–2649 (1997).
- [3] Santarelli, G. *et al.* Quantum projection noise in an atomic fountain: A high stability cesium frequency standard. *Phys. Rev. Lett.* **82**, 4619 (1999).
- [4] Takamoto, M., Hong, F.-L., Higashi, R. & Katori, H. An optical lattice clock. *Nature* **435**, 321–324 (2005).
- [5] Santra, R., Arimondo, E., Ido, T., Greene, C. H. & Ye, J. High-accuracy optical clock via three-level coherence in neutral bosonic ^{88}Sr . *Phys. Rev. Lett.* **94**, 173002 (2005).
- [6] Fixler, J. B., Foster, G. T., McGuirk, J. M. & Kasevich, M. A. Atom interferometer measurement of the Newtonian constant of gravity. *Science* **315**, 74–77 (2007).
- [7] Ye, J., Kimble, H. J. & Katori, H. Quantum state engineering and precision metrology using state-insensitive light traps. *Science* **320**, 1734–1738 (2008).
- [8] Wineland, D. J., Bollinger, J. J., Itano, W. M., Moore, F. L. & Heinzen, D. J. Spin squeezing and reduced quantum noise in spectroscopy. *Phys. Rev. A* **46**, R6797 (1992).
- [9] Wineland, D. J., Bollinger, J. J., Itano, W. M. & Heinzen, D. J. Squeezed atomic states and projection noise in spectroscopy. *Phys. Rev. A* **50**, R67 (1994).
- [10] Xiao, M., Wu, L.-A. & Kimble, H. J. Precision measurement beyond the shot-noise limit. *Phys. Rev. Lett.* **59**, 278–281 (1987).
- [11] Kitagawa, M. & Ueda, M. Squeezed spin states. *Phys. Rev. A* **47**, 5138 (1993).
- [12] Wiseman, H. M. Quantum theory of continuous feedback. *Phys. Rev. A* **49**, 2133 (1994).
- [13] Kuzmich, A., Bigelow, N. P. & Mandel, L. Atomic quantum non-demolition measurements and squeezing. *Europhys. Lett.* **42**, 481–486 (1998).
- [14] Hald, J., Sørensen, J. L., Schori, C. & Polzik, E. S. Spin squeezed atoms: A macroscopic entangled ensemble created by light. *Phys. Rev. Lett.* **83**, 1319 (1999).
- [15] Meyer, V. *et al.* Experimental demonstration of entanglement-enhanced rotation angle estimation using trapped ions. *Phys. Rev. Lett.* **86**, 5870–5873 (2001).
- [16] Julsgaard, B., Kozhokin, A. & Polzik, E. S. Experimental long-lived entanglement of two macroscopic objects. *Nature* **413**, 400–403 (2001).
- [17] Sørensen, A. S. & Mølmer, K. Entanglement and extreme spin squeezing. *Phys. Rev. Lett.* **86**, 4431–4434 (2001).
- [18] Bouchoule, I. & Mølmer, K. Preparation of spin-squeezed atomic states by optical-phase-shift measurement. *Phys. Rev. A* **66**, 043811 (2002).
- [19] Leibfried, D. *et al.* Toward Heisenberg-limited spectroscopy with multiparticle entangled states. *Science* **304**, 1476–1478 (2004).
- [20] André, A., Sørensen, A. S. & Lukin, M. D. Stability of atomic clocks based on entangled atoms. *Phys. Rev. Lett.* **92**, 230801 (2004).
- [21] Orzel, C., Tuchman, A. K., Fenselau, M. L., Yasuda, M. & Kasevich, M. A. Squeezed states in a Bose-Einstein condensate. *Science* **291**, 2386 (2001).
- [22] Jo, G.-B. *et al.* Long phase coherence time and number squeezing of two Bose-Einstein condensates on an atom chip. *Phys. Rev. Lett.* **98**, 030407 (2007).
- [23] Kuzmich, A., Mandel, L. & Bigelow, N. P. Generation of spin squeezing via continuous quantum nondemolition measurement. *Phys. Rev. Lett.* **85**, 1594 (2000).
- [24] Takano, T., Fuyama, M., Namiki, R. & Takahashi, Y. Spin squeezing of a cold ensemble with the nuclear spin of one-half (2008). [arXiv:quant-ph/0808.2353v1](https://arxiv.org/abs/quant-ph/0808.2353v1).
- [25] Estève, J., Gross, C., Weller, A., Giovanazzi, S. & Oberthaler, M. K. Squeezing and entanglement in a bose-einstein condensate. *Nature* (2008). URL <http://www.nature.com/nature/journal/vaop/ncurrent/abs/nature07332.html>. Advance online publication.
- [26] Chaudhury, S. *et al.* Quantum control of the hyperfine spin of a Cs atom ensemble. *Phys. Rev. Lett.* **99**, 163002 (2007).
- [27] Teper, I., Vrijsen, G., Lee, J. & Kasevich, M. A. Backaction noise produced via cavity-aided nondemolition measurement of an atomic clock state (2008). [arXiv:quant-ph/0807.4762v1](https://arxiv.org/abs/quant-ph/0807.4762v1).
- [28] Harber, D. M., Lewandowski, H. J., McGuirk, J. M. & Cornell, E. A. Effect of cold collisions on spin coherence and resonance shifts in a magnetically trapped ultracold gas. *Phys. Rev. A* **66**, 053616 (2002).
- [29] Treutlein, P., Hommelhoff, P., Steinmetz, T., Hänsch, T. W. & Reichel, J. Coherence in microchip traps. *Phys. Rev. Lett.* **92**, 203005 (2004).
- [30] Sortais, Y. *et al.* Cold collision frequency shifts in a ^{87}Rb atomic fountain. *Phys. Rev. Lett.* **85**, 3117–3120 (2000).
- [31] Appel, J. *et al.* Submitted to Nature Physics simultaneously with this work.

Reduced-Quantum-Uncertainty States for an Atomic Clock: Supplementary Methods

Monika H. Schleier-Smith, Ian D. Leroux, and Vladan Vuletić*

Department of Physics, MIT-Harvard Center for Ultracold Atoms, and Research Laboratory of Electronics, Massachusetts Institute of Technology, Cambridge, Massachusetts 02139, USA

(Dated: May 8, 2022)

We present a detailed description of the interactions between atoms, light, and optical resonator essential to our experiment. Section III gives the relevant physical parameters of the resonator. Section IV describes the optical dipole trap used to confine the atomic cloud in the resonator, which determines the cloud geometry and thus the coupling of the atoms to the resonator mode. Section V describes the loading of the atoms into this trap. Section VI presents the probe laser and detection scheme, while section VII explains how the measurements are interpreted in terms of atom number. Section VIII presents a measurement of the probe-induced phase shift on the atoms, an independent experimental confirmation of our good understanding of the atom-light interaction. The spin echo technique we use to suppress the undesirable effects of this phase shift is explained in section IX. The effects of scattering into free space, which set the fundamental limit to the performance of our scheme, are presented in section X. Finally, in section XI we elaborate on the determination of spin noise suppression and of contrast loss, as the balance between these two factors determines the squeezing parameters that constitute the central result of this work.

III. OPTICAL RESONATOR

Our near-confocal Fabry-Pérot resonator, which serves to enhance the quantum non-demolition (QND) measurement, has a measured free spectral range of $\omega_{\text{FSR}} = 2\pi \times 5632.0(2)$ MHz and a transverse mode spacing of $\omega_{\text{trans}} = 2\pi \times 226(2)$ MHz. From these we compute a mirror separation of $L = \pi c/\omega_{\text{FSR}} = 26.62(1)$ mm, a resonator g parameter[1] of $g = \cos(\frac{\pi}{2}(\omega_{\text{trans}}/\omega_{\text{FSR}} + 1)) = -0.0629(6)$ (assuming symmetric mirrors), and a mirror curvature radius $R = L/(1 - g) = 25.04(2)$ mm.

At the probe wavelength of the rubidium D_2 transition, $\lambda_p = 780$ nm, the observed cavity linewidth is $\kappa_{780} = 2\pi \times 1.01(3)$ MHz, so that the cavity finesse is $F_{780} = \omega_{\text{FSR}}/\kappa_{780} = 5.6(2) \times 10^3$. The mirrors are transmission-dominated at this wavelength: the observed finesse corresponds to a single-mirror power transmission of $5.6(2) \times 10^{-4}$, whereas the scattering and absorption losses are $\sim 5 \times 10^{-5}$. The atom cloud is longitudinally displaced by $z_{\text{atoms}} = 2.6(5)$ mm from the cavity center, as observed by absorption imaging of the trapped atoms. Thus the resonator mode waist for λ_p at the atoms' location is $w = w_0 \sqrt{1 + (z_{\text{atoms}}/z_R)^2} = 56.9(4)$ μm , where $z_R = \pi w_0^2/\lambda$ is the Rayleigh range and $w_0 = \frac{L\lambda}{2\pi} \sqrt{(1+g)/(1-g)}$ is the mode waist at cavity center.

The resulting single-atom cooperativity[2]—defined for a two-level atom located on the cavity axis at an antinode of the standing wave—is $\eta_0 = 24F/\pi(kw)^2 = 0.203(7)$.

At the wavelength $\lambda_t = 851$ nm used for the optical dipole trap, the mode waist at the atoms' location, computed from the same mirror geometry as above, is $w = 59.5(5)$ μm . The measured cavity linewidth is $\kappa_{851} = 2\pi \times 135(2)$ kHz, giving a finesse $F_{851} = 4.2(1) \times 10^4$. The mirror power transmission at λ_t , measured directly for an identical mirror, is $2.7(2) \times 10^{-5}$. We infer the intracavity dipole trap power from the transmitted power using this transmission fraction.

IV. OPTICAL DIPOLE TRAP

The atoms are confined in the wells of a standing-wave dipole trap formed by an 851-nm DFB laser locked to a TEM₀₀ mode of the optical resonator using the Pound-Drever-Hall technique[3]. The lock bandwidth is 1 MHz and the resulting fractional trap power noise density is $6 \times 10^{-6}/\sqrt{\text{Hz}}$ at 1 kHz and falls off rapidly above the cavity linewidth. This noise is sufficiently low that parametric heating is negligible.

The circulating power $P_1 = 3.5$ W yields a trap depth $U_0 = \frac{P_1}{\pi w^2 I_s} \frac{\hbar \Gamma^2}{|\Delta_{\text{eff}}|} = h \times 24$ MHz. Here, $\Delta_{\text{eff}} = 3/(2\Delta_{D_2}^{-1} + \Delta_{D_1}^{-1}) = -2\pi \times 29.3$ THz is an effective detuning from the D_1 and D_2 optical transitions, while the ratio of the squared excited state linewidth to the saturation intensity is $\Gamma^2/I_s = (2\pi)^2 \times 2.2 \times 10^{12}$ Hz²m²/W for both lines. The radial and axial trap frequencies are, respectively, $\omega_r = \sqrt{4U_0/(mw^2)} = 2\pi \times 1.8$ kHz and $\omega_{\text{ax}} = \sqrt{4U_0 E_r^{851}/h} = 2\pi \times 550$ kHz, with E_r^{851} the recoil energy of ⁸⁷Rb at 851 nm.

The axial temperature of the atoms causes them to move away from the longitudinal maximum of the standing-wave intensity profile of the trap, weakening their radial confinement. We measure a radial trap half-period of $t_{1/2} = 330(20)$ μs (see section IX), indicating an effective trap depth for the radial motion of $U_0 - k_B T_{\text{ax}} = h \times 18(2)$ MHz. From this we infer an axial temperature $k_B T_{\text{ax}} = h \times 6(2)$ MHz. The radial temperature is measured by suddenly releasing the trap and observing the ballistic radial expansion of the cloud as a decrease in coupling to the resonator. This yields a radial temperature of $k_B T_{\text{rad}} = h \times 1.3(2)$ MHz. The RMS radius of the cloud is $\sigma = (t_{1/2}/\pi) \sqrt{k_B T_{\text{rad}}/m} = 8.1(8)$ μm , which is much less than the cavity mode waist. Axially, the cloud is ~ 1 mm (~ 2000 wells) long. This is much longer than

the 4.7 μm period of the spatial beating between the trap and probe standing waves, so that the atoms are evenly distributed over all longitudinal positions relative to the probe's standing wave profile.

To minimize inhomogeneous broadening of the clock transition, the trap light is elliptically polarized such that the vector light shift cancels, to lowest order, the differential scalar light shift of the clock states. Such a cancellation is possible because the vector light shift acts as an effective magnetic field [4] and can be added to a real magnetic field to yield a quadratic Zeeman shift which, like the scalar light shift, is linear in the local intensity of trap light. In particular, in a magnetic field B_z along the resonator axis, for an atom at potential $U < 0$ in the dipole trap, the $|F = 1, m_F = 0\rangle \rightarrow |F = 2, m_F = 0\rangle$ transition frequency is shifted by

$$\frac{\delta(U)}{2\pi} = -\frac{\omega_{\text{HF}}}{\Delta_{\text{eff}}} \frac{U}{h} + \beta \left(B_z + f b_{\sigma_+} \frac{U}{h} \right)^2, \quad (2)$$

where $\omega_{\text{HF}} = 2\pi \times 6.835$ GHz is the ground-state hyperfine splitting, $\beta = 574$ Hz/G² sets the scale of the quadratic Zeeman shift[5], the coefficient $b_{\sigma_+} = (\Delta_{\text{D}_1}^{-1} - \Delta_{\text{D}_2}^{-1})\Delta_{\text{eff}} \times h/3\mu_B = 0.061$ G/MHz gives the effective magnetic field per unit trap depth for σ_+ -polarized light, and f is the circular polarization fraction of the trap light. The broadening is minimized by choosing a combination of B_z and f that places the minimum of the parabola described by Eq. 2 at $U = -U_0 + k_B T_{\text{ax}}$. At our field of $B_z = 5.6$ G, we find an optimum circular polarization fraction $f = 0.5(1)$. For our axial temperature $k_B T_{\text{ax}}/h = 6(2)$ MHz, the residual broadening is $\beta(f b_{\sigma_+} k_B T_{\text{ax}})^2 = 20$ Hz, consistent with our measured 10(2) ms coherence time.

V. EXPERIMENT CYCLE

The experiment cycle begins with a 5 s loading stage in which ⁸⁷Rb atoms from a background vapor are collected, cooled and trapped in a conventional six-beam magneto-optical trap (MOT). The atoms are transferred to a quadrupole magnetic trap which is then ramped up toward a microchip. The field produced by the chip wires[6] deforms the trap into an elongated geometry matched to the cavity mode, which runs parallel to the chip surface at a distance of 200 μm . The dipole trap power is then turned up, capturing the atoms at the antinodes of its intracavity standing wave, and the magnetic trap is turned off. After additional polarization gradient cooling, the dipole-trapped atoms are optically pumped into the $|F = 1, m_F = 0\rangle$ clock state which serves as the starting point for subsequent measurements.

Since the trap light must be linearly polarized for polarization gradient cooling, which relies on all m_F sub-levels being degenerate, the optimal elliptical polarization to minimize inhomogeneous broadening is introduced after the cooling step with a variable retarder.

VI. DETECTION SETUP

We probe on the D₂ transition through the optical cavity with linear polarization, measuring the shift in the cavity resonance due to the atoms' index of refraction. The probe laser, like the trap laser (see section IV), is locked to the resonator via a Pound-Drever-Hall lock of 1 MHz bandwidth. A feedback loop based on the beat frequency between the probe laser and a reference laser (locked via Doppler-free spectroscopy to an atomic transition in ⁸⁵Rb) stabilizes the resonator frequency.

The cavity is tuned such that the probe laser carrier lies halfway between two TEM₀₀ modes of the resonator. A broadband electro-optic modulator (model PM-0K5-10-PFA-PFA-780-UL from EOSPACE) is used to phase-modulate the probe laser with sidebands for locking and probing (see Fig. S5). A lock sideband at 113 MHz is resonant with the TEM₁₀ mode, producing the Pound-Drever-Hall error signal. The RMS frequency fluctuations on the lock are 2×10^{-3} of the resonator linewidth in our measurement bandwidth of 5 kHz.

The probe sideband at $(5\omega_{\text{FSR}} + \kappa)/2 \approx 2\pi \times 14080$ MHz lies on the slope of a TEM₀₀ resonances with a detuning of $+2\pi \times 3.57(1)$ GHz relative to the atomic $F = 2 \rightarrow F' = 3$ transition. The symmetric sideband at $-(5\omega_{\text{FSR}} + \kappa)/2$, far off-resonant from the atoms, lies on the opposite slope of another TEM₀₀ mode, such that the total transmission in the two TEM₀₀ modes is sensitive only to differential cavity shifts, as induced by the atoms, and not to common-mode shifts, such jitter of the laser relative to the cavity. We refer to this last sideband as the compensation sideband.

The transmitted power in the TEM₀₀ mode is coupled into a single-mode fiber, which spatially filters out the lock sideband, and subsequently detected with overall quantum efficiency $Q_e = 0.43(4)$ on a Si avalanche photodiode (Hamamatsu model S3884) operating at an avalanche gain $M = 13$. At a typical power of 2 nW, our detection is limited by photocurrent noise augmented by the excess noise of the avalanche photodiode, which is a factor of 1.9 in variance above the photocurrent shot noise.

VII. ATOM NUMBER CALIBRATION

In calibrating atom projection noise and squeezing below atom projection noise we rely on, respectively, accurate measurement of atom number and precise measurement of population difference between the clock states.

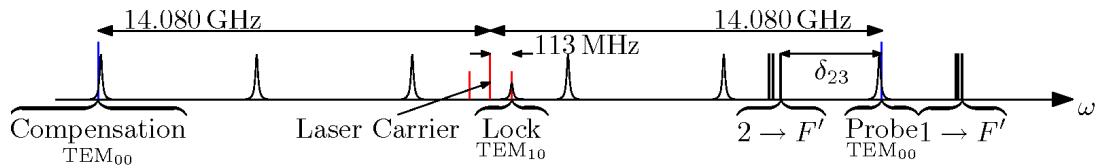


FIG. S5: **Laser stabilization and detection scheme**, indicating frequencies of carrier and lock sidebands (red) and probe and compensation sidebands (blue) relative to cavity resonances and atomic transitions. Not to scale.

A. Atom Number Measurement and Effective Atom Number

The quantity we measure directly in our experiment is the optical depth

$$OD = 2N_{\text{tot}}\bar{\eta} = 2 \int n(\rho, z)\eta(\rho, z) dV, \quad (3)$$

of the ensemble of N_{tot} atoms spatially distributed with density $n(\rho, z)$, where $\eta(\rho, z)$ is the spatially dependent single-atom cooperativity. $\eta(\rho, z)$ is proportional to the local intensity of the probe light, which forms a standing wave incommensurate with that in which the atoms are trapped. We obtain the optical depth from the atom-induced shift of the cavity resonance:

$$\omega_F = \frac{N_{\text{tot}}\bar{\eta}\Gamma\kappa}{6\delta_F} \quad (4)$$

for σ_+/σ_- -polarized light probing atoms in hyperfine state F , with δ_F the detuning of the cavity resonance from the $|5^2S_{1/2}, F\rangle \rightarrow |5^2P_{3/2}, F'\rangle$ transitions, averaged over final states F' . This formula is valid under the assumption that δ_F is large compared to the excited-state hyperfine splitting, and that the sublevels m_F and $-m_F$ are equally populated (i.e. no net magnetization of the sample along z).

Because of the unequal coupling of different atoms to the probe light (e.g. atoms at nodes are completely uncoupled), the total atom number in the cloud N_{tot} is not an especially useful quantity for describing our system. Rather, we define an effective atom number

$$N_0 \equiv \frac{4}{3}N_{\text{tot}}\bar{\eta}/\eta_0 = \frac{8\delta_F}{\eta_0\Gamma} \frac{\omega_F}{\kappa}. \quad (5)$$

The numerical prefactor is chosen such that the projection noise variance of the effective atom number for an ensemble of atoms uniformly distributed along the resonator axis satisfies the usual projection-noise relation

$$\frac{(\Delta N)^2}{N_0} = \frac{(4/3)^2 \int_0^{2\pi} \sin^4(kz) dz}{(4/3) \int_0^{2\pi} \sin^2(kz) dz} = 1, \quad (6)$$

which avoids carrying an uninteresting factor of 3/4 through the equations and allows direct comparison to a spatially uniform system. The radial extent of our cloud introduces a small correction to equation 6, which will be

discussed in section VII C. For our cloud geometry, one effective atom corresponds to 1.62(2) real atoms. Note that the effective atom number N_0 is proportional to the measured cavity shift by a factor which depends only on the atomic linewidth, the probe detuning, and well-characterized cavity parameters (see section III).

B. Measurement of S_z Near $S_z = 0$

As described in Section VI, the probe and compensation sidebands are placed on opposite slopes of two cavity resonances, such that the cavity transmission is a direct measure of the differential shift $\omega = \omega_{\text{probe}} - \omega_{\text{comp.}}$ of these two resonances. The probe sideband is tuned to the frequency between the $|5^2S_{1/2}, F = 1\rangle \rightarrow |5^2P_{3/2}\rangle$ and $|5^2S_{1/2}, F = 2\rangle \rightarrow |5^2P_{3/2}\rangle$ transitions for which ω has the same magnitude—and opposite sign—for atoms in $F = 1$ and $F = 2$:

$$\begin{aligned} \omega_{\text{probe}} - \omega_{\text{comp.}} &= \frac{\eta_0\Gamma\kappa}{8} \left[N_2 \left(\frac{1}{\delta_2^{\text{probe}}} - \frac{1}{\delta_2^{\text{comp.}}} \right) \right. \\ &\quad \left. + N_1 \left(\frac{1}{\delta_1^{\text{probe}}} - \frac{1}{\delta_1^{\text{comp.}}} \right) \right] \\ &= \frac{(N_2 - N_1)\eta_0\Gamma\kappa}{8\delta'} \end{aligned} \quad (7)$$

where N_F is the effective atom number in hyperfine state F , $\delta_F^{\text{comp.}} = \delta_F^{\text{probe}} - 5\omega_{\text{FSR}} - \kappa$, and $\delta' = 2\pi \times 3200(10)$ MHz. See Table S1 for details of the mode shifts and their uncertainties. The resulting differential shift is $d\omega/dN = 2\pi \times 48(2)$ Hz/atom. The sidebands are detuned by $\pm\kappa/2$ from their respective resonances when $S_z = 0$. Fluctuations in total atom number and projection noise on N both leave the sidebands well in the linear regime of the Lorentzian transmission profiles. Thus, the total transmission of the probe and compensation sidebands is

$$P_p + P_c = P_0 \left(1 + \frac{N\eta_0\Gamma}{8\delta'} \right), \quad (8)$$

where P_0 is the transmission of a single sideband on resonance. Monitoring fractional changes in the transmitted power provides a sensitive measure of $S_z = N/2$ for states near the equator of the Bloch sphere.

Resonance	$\delta_{23}/(2\pi \text{ GHz})$	Cavity Shift per Effective Atom/ $(\kappa \times 10^{-6})$	
		$ F = 1, m_F = 0\rangle$	$ F = 2, m_F = 0\rangle$
Probe	3.57(1)	-53(2)	+42(1)
Lock	-10.40(1)	-0.7(1)	-1.1(2)
Compensation	-24.59(1)	-5.0(2)	-6.3(2)

TABLE S1: **Atom-induced frequency shifts for relevant resonator modes.** δ_{23} is the detuning of the given mode from the $5^2S_{1/2}, F = 2 \rightarrow 5^2P_{3/2}, F' = 3$ atomic transition. The shifts are expressed in millionths of a cavity linewidth for one effective atom in either of the two clock states. The calculated shifts include the full excited state hyperfine structure as well as the reduced spatial overlap with the TEM₁₀ lock resonance for our cloud size.

C. Measurement of N_0 and Verification of Projection Noise

The atom number N_0 is calibrated by first optically pumping the sample into $F = 2$, then depumping all atoms into $F = 1$ and measuring the change in shift of the probe resonance. Since typical atom numbers shift the resonance by a linewidth or more, the determination of atom number relies on measurements in the wings of the Lorentzian transmission profile and thus incurs greater uncertainty than do measurements of S_z near the equator of the Bloch sphere, for which we achieve sub-projection noise resolution.

Nevertheless, having absolute measures both of atom projection noise and of atom number, we are able to verify their consistency. The projection noise variance of N should satisfy, for a state with expectation values $\langle N_1 \rangle = \langle N_2 \rangle = N_0/2$,

$$\begin{aligned}
 a^c &= \frac{(\Delta N)^2}{N_0} = \frac{4}{3\eta_0} \frac{\int n(\rho, z)[\eta(\rho, z)]^2 dV}{\int n(\rho, z)\eta(\rho, z) dV} \\
 &= \frac{\int_0^\infty e^{-\rho^2/2\sigma^2 - 4\rho^2/w^2} 2\pi\rho d\rho}{\int_0^\infty e^{-\rho^2/2\sigma^2 - 2\rho^2/w^2} 2\pi\rho d\rho} \\
 &= \frac{w^2 + 4\sigma^2}{w^2 + 8\sigma^2} = 0.93(1), \quad (9)
 \end{aligned}$$

In factoring out the axial integral, we have used the fact that the cloud is many wavelengths long but the mode waist is essentially constant—varying by only 1%—over the length of the cloud.

A linear fit to the measured projection noise versus N_0 gives a slope of 1.1(1) (Fig. 2 of the main text). However, the data are also consistent with the predicted projection noise slope of 0.93 combined with a small quadratic term due to fractional technical noise. Since the measurement of projection noise relies on comparing two states independently prepared by $\pi/2$ pulses, we attribute this noise to microwave power fluctuations of 0.3(1)% between the two preparations. In calculating squeezing parameters, we conservatively take the atom projection noise to be that of equation 9, not the slightly larger measured noise which would make the squeezing criteria easier to fulfill.

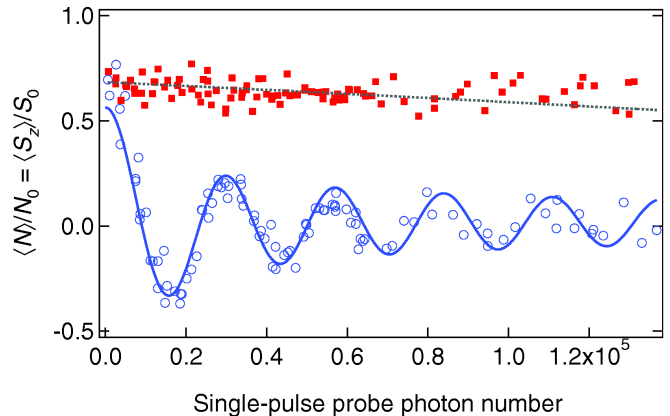


FIG. S6: **Measurement of the atom-photon interaction.** A probe pulse of varying photon number p is inserted into a Ramsey sequence. The observed oscillation of the atomic phase (blue open circles) is due to the differential light shift between atomic states, while the damping is due to the inhomogeneity of this light shift. The light-induced phase shift and decoherence can be suppressed by a spin echo technique where a microwave π pulse is inserted between two probe pulses (red solid squares). They grey dotted line is the fit to the contrast data of Fig. 4, discussed in section XI B.

VIII. EXPERIMENTAL VERIFICATION OF THE ATOM-CAVITY INTERACTION

The dispersive shift of the cavity resonance by the atom is dual to the Stark shift of the atomic energies by intracavity photons. The symmetry between these effects is best seen in the dressed-state picture, where they correspond to the repulsion of states with an excitation in either the atom or the cavity, coupled by the atom-light interaction. The Stark shift can be parametrized by the phase induced between the $|F = 1, m_F = 0\rangle$ and $|F = 2, m_F = 0\rangle$ states of an atom located on the cavity axis at an antinode when p probe photons are transmitted through the cavity. From the preceding cavity parameters we compute this to be $p\phi_1 = p(\eta_0\Gamma/3)(\delta_2^{-1} - \delta_1^{-1}) = p \times 253(8) \mu\text{rad}$. We ignore the phase shifts due to lock and compensation light as the increased detuning and decreased spatial overlap with the probing mode suppresses them by a factor of more than 20.

We are able to verify the value of ϕ_1 experimentally by means of a Ramsey measurement[7], applying an optical probe pulse of variable duration between the microwave $\pi/2$ pulses and then detecting the population difference $2S_z$ via the resonator shift. This measurement is performed at sufficiently small atom number ($N_0 = 3 \times 10^3$) that the backaction of the atoms on the measurement can be neglected. The Ramsey signal, shown in Fig. S6, is an oscillatory function of the photon number transmitted through the resonator that is damped due to inhomogeneous light shifts. For an ensemble of atoms on the resonator axis evenly distributed with respect to the probe standing wave, a spin state prepared on the x -axis of the Bloch sphere will, after exposure to p probe photons, have

$$\begin{aligned} \langle S_x \rangle &\propto \frac{\int_0^{2\pi} \cos(p\phi_1 \sin^2(kz)) \sin^2(kz) dz}{\int_0^{2\pi} \sin^2(kz) dz} \\ &= J_0\left(\frac{p\phi_1}{2}\right) \cos\left(\frac{p\phi_1}{2}\right) \\ &\quad - J_1\left(\frac{p\phi_1}{2}\right) \sin\left(\frac{p\phi_1}{2}\right), \end{aligned} \quad (10)$$

where the J_n are Bessel functions of the first kind. From a fit of this form (shown in Fig. S6), we extract $\phi_1 = 230(20) \mu\text{rad}$. A full numerical model including the radial cloud size yields $\phi_1 = 250(20) \mu\text{rad}$, in excellent agreement with the value derived from cavity parameters. This experimentally confirms our quantitative understanding of the atom-cavity interaction.

IX. SUPPRESSING PROBE-INDUCED DEPHASING: SPIN ECHO SEQUENCE

The large light-induced dephasing between the atomic spins evident in Fig. S6 corresponds to a reduction of the ensemble spin S that would be prohibitive for spin squeezing. Fortunately, the coherence reduction can be reversed by a spin echo technique. In particular, we always apply probe light in two $50 \mu\text{s}$ pulses separated by a composite π pulse. The composite π pulse $R_{\pi/3}(\pi)R_{-\pi/3}(\pi)R_{\pi/3}(\pi)$ consists of three simple microwave π pulses, where the subscripts indicate phases chosen to compensate imperfections of the microwave pulse length or intensity[8]. To ensure that each atom experiences the same probe intensity during the rephasing pulse as during the dephasing pulse, the probe pulses are separated by half the radial trap period. We find the optimal pulse separation to be $330(20) \mu\text{s}$, which we take to be a measurement of the half-period of radial oscillation in the trap.

This echo sequence substantially reduces the probe-induced decoherence, as evidenced by the small slope of the corresponding red data points in Fig. S6. The spin echo technique removes the detrimental effects of the inhomogeneous atom-light interaction, since the final atomic state depends only on the net phase incurred, but

does not compromise our spin squeezing measurement of S_z , since we record the transmission of the two probe pulses separately.

X. EFFECTS OF SCATTERING INTO FREE SPACE

All photons scattered into free space can in principle be associated with a particular scattering atom. To the extent that they reveal the state of that atom, they project it into either the upper or lower clock state (or, given that this information is not recorded, a statistical mixture of the two) with no coherence between them. Including the various possible Raman scattering processes on the D_2 line, all of which reveal the state of the scattering atom, and the slight difference in Rayleigh scattering rates, which conveys partial information about the state of the scatterer[9], we find that the fractional loss of contrast is $3.6(2) \times 10^{-8}$ per probe photon exiting the cavity. The effect of lock and compensation photons is two orders of magnitude smaller. At our chosen photon number for squeezing of 5×10^5 this corresponds to a 1.8% effect, which is much smaller than our observed contrast loss.

In addition to loss of contrast, certain Raman scattering processes can add to our measurement noise. If the hyperfine state of some set of atoms is changed by Raman scattering events near the end of the squeezing measurement or the beginning of the readout measurement, the squeezing and readout measurements of the same atomic sample will differ by twice the number of flipped atoms and the fluctuations in this difference will add to our observed measurement noise. We expect to see a scattering-induced variance of $5.7(2) \times 10^{-8}$ of the effective atoms per probe photon exiting the cavity. The lock and compensation sideband contributions are again suppressed by two orders of magnitude by a combination of detuning and spatial mode-matching. For $p = 5 \times 10^5$, the variance added by this process corresponds to 2.8% of our effective atoms, which would only be noticeable at a measurement sensitivity 15 dB below the shot noise limit.

The fact that scattering effects are still negligible in our experiment indicates that, provided the current technical limits can be overcome, much greater squeezing can be achieved.

XI. DETERMINATION OF SQUEEZING PARAMETER CONSTITUENTS

The squeezing parameters shown in Fig. 4 are derived, as explained in the main text, from the spin noise suppression $(\Delta S_z)^2 / (\Delta S_z)_{\text{CSS}}^2$ and the contrast \mathcal{C} . Here, we elaborate on our determination of these two quantities.

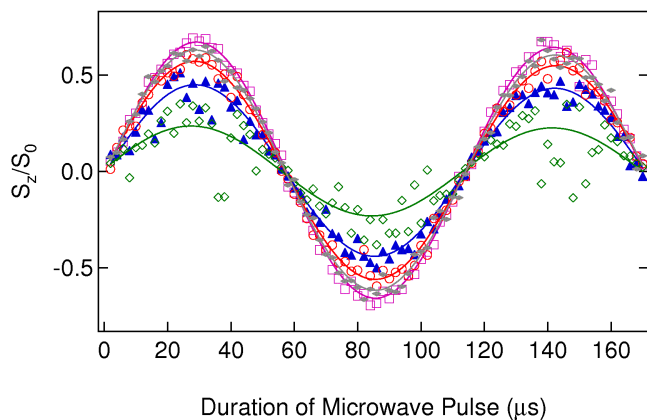


FIG. S7: **Rabi oscillation data with fit curves used to determine contrast.** The open magenta squares correspond to Rabi oscillations driven after applying only lock light but no probe light, so that the magenta curve has contrast C_{initial} . Each of the successively smaller curves, taken at photon numbers ranging from 1×10^5 to 9×10^5 , gives rise to a contrast data point in Fig. 4 (open grey squares).

A. Spin Noise Suppression

A measurement with uncertainty $(\delta S_z)^2$, combined with prior knowledge of S_z with uncertainty $(\Delta S_z)_{\text{CSS}}^2 = aS_0/2$, reduces the spin noise to

$$(\Delta S_z)^2 = \left(\frac{1}{(\Delta S_z)_{\text{CSS}}^2} + \frac{1}{(\delta S_z)^2} \right)^{-1}. \quad (11)$$

Hence, the spin noise suppression is given by

$$\frac{(\Delta S_z)^2}{(\Delta S_z)_{\text{CSS}}^2} = \frac{(\delta S_z)^2}{(\delta S_z)^2 + aS_0/2}. \quad (12)$$

Here, a is the prefactor calculated in section VII C that accounts for the spatially inhomogeneous atom-probe coupling associated with the radial extent of the atom cloud. Each spin noise suppression value plotted in Fig. 4 (blue open diamonds) is obtained, using Eq. 12, from the measurement uncertainty $(\delta S_z)^2$ from Fig. 2 inset (blue

solid diamonds) and the CSS spin noise $aS_0/2$ (dashed red line in Fig. 2 inset) calculated from the measured atom number $N_0 = 2S_0$.

B. Contrast

The open grey squares in Fig. 4 show the clock contrast remaining after applying p probe photons in our usual measurement procedure. Each data point corresponds to the amplitude of a Rabi oscillation curve constructed from a series of shots in which we apply after the probe pulses a microwave pulse of variable duration and subsequently read out S_z . The set of Rabi oscillation curves (Fig. S7) shows that there are two distinct mechanisms contributing to contrast loss. One reduces the length $|\mathbf{S}|$ of the Bloch vector, as evidenced by the reduction in amplitude of the envelope, while another imparts shot-to-shot fluctuations in phase, visible as an increased spread of the data points under the envelope. The reduction in $|\mathbf{S}|$ is linear in probe power. Although not yet completely understood, we believe it to be due to the thermal motion of the atoms in the trap, which leads to an imperfect cancellation in the spin echo sequence and residual inhomogeneous dephasing. The shot-to-shot phase fluctuations arise from imbalances in the intracavity probe power between the two spin echo pulses due to photon shot noise and additional technical noise. The onset of the associated reduction in $|\langle \mathbf{S} \rangle|$ is only quadratic in the phase broadening and hence in probe photon number. Describing the contrast loss by

$$\frac{dC}{dp} = -\alpha C - \beta p C, \quad (13)$$

we fit to the data the dotted grey curve

$$C = C_{\text{in}} e^{-\alpha p - \beta p^2/2}, \quad (14)$$

obtaining $\alpha = 7(1) \times 10^{-7}$, $\beta = 9(4) \times 10^{-13}$, and $C_{\text{in}} = 0.69(1)$. The poor initial contrast C_{in} is due to the light required to lock the probe laser to the resonator and can be improved by detuning the lock light further from atomic resonance.

[1] Siegman, A. E. *Lasers* (University Science Books, Sausalito, 1986).
 [2] Vuletić, V., Chan, H. W. & Black, A. T. Three-dimensional cavity Doppler cooling and cavity sideband cooling by coherent scattering. *Phys. Rev. A* **64**, 033405 (2001).
 [3] Drever, R. W. P. *et al.* Laser phase and frequency stabilization using an optical resonator. *Applied Physics B* **31**, 97–105 (1983).
 [4] Deutsch, I. H. & Jessen, P. S. Quantum-state control in optical lattices. *Phys. Rev. A* **57**, 1972–1986 (1998).

[5] Vanier, J. & Audoin, C. *The Quantum Physics of Atomic Frequency Standards* (Hilger, Philadelphia, 1989).
 [6] Lin, Y., Teper, I., Chin, C. & Vuletić, V. Impact of Casimir-potential and Johnson noise on Bose-Einstein condensate stability near surfaces. *Phys. Rev. Lett.* **92**, 050404 (2003).
 [7] Ramsey, N. F. A molecular beam resonance method with separated oscillating fields. *Phys. Rev.* **78**, 695 (1950).
 [8] Vandersypen, L. M. K. & Chuang, I. L. NMR techniques for quantum control and computation. *Rev. Mod. Phys.* **76**, 1037–1069 (2005).

- [9] Ozeri, R. *et al.* Hyperfine coherence in the presence of spontaneous photon scattering. *Phys. Rev. Lett.* **95**, 030403 (2005).